Journal of Colloid and Interface Science 596 (2021) 493–499

Contents lists available at ScienceDirect

Journal of Colloid and Interface Science

journal homepage: www.elsevier.com/locate/jcis

Regular Article

Axisymmetric bare freestanding films of highly viscous liquids: Preparation and real-time investigation of capillary leveling

Vincenzo Ferraro [a,b,1], Massimiliano M. Villone [a,b,1], Volodymyr Tkachenko [c,b], Lisa Miccio [b,c], Lorenzo Lombardi [a,b], Daniele Tammaro [a,b], Ernesto Di Maio [a,b], Gaetano D'Avino [a,b], Pier Luca Maffettone [a,b,*]

[a] Dipartimento di Ingegneria Chimica, dei Materiali e della Produzione Industriale, Università degli Studi di Napoli Federico II, Piazzale Tecchio 80, 80125 Napoli, Italy
[b] NEAPoLIS, Numerical and Experimental Advanced Program on Liquids and Interface Systems, Joint Research Center CNR - Università degli Studi di Napoli Federico II, Piazzale Tecchio 80, 80125 Napoli, Italy
[c] CNR-ISASI, Institute of Applied Sciences and Intelligent Systems E. Caianiello, Via Campi Flegrei 34, 80078 Pozzuoli, Napoli, Italy

GRAPHICAL ABSTRACT

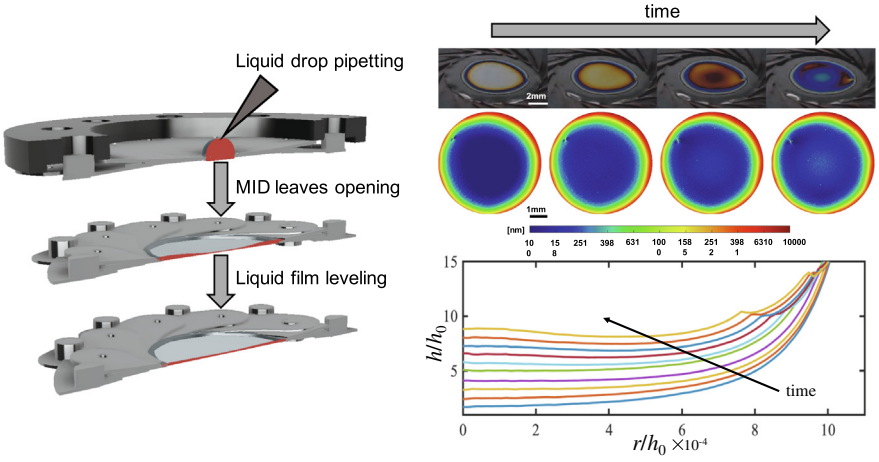

ARTICLE INFO

Article history:
Received 13 March 2021
Accepted 18 March 2021
Available online 27 March 2021

Keywords:
Axisymmetric bare freestanding liquid films
Capillary leveling flow
Opto-mechanical device
Direct numerical simulations
Lubrication theory

ABSTRACT

Hypothesis: Thin liquid films are important in many scientific fields. In particular, films with both the surface layers exposed to a different fluid phase, known as freestanding films, are relevant in the ambit of foams and emulsions. Hence, there is a great interest in developing novel techniques allowing to form large and stable freestanding liquid films and to follow their dynamics.

Experiments: We develop a novel opto-mechanical tool allowing to perform and study the preparation and the capillary leveling flow of axisymmetric bare freestanding liquid films. The tool is composed by a customized motorized iris diaphragm and by an innovative joint imaging setup combining digital holography and white light color interferometry that enables real-time measurement of film thickness over a large field of view. The dynamics of films made of a model Newtonian fluid, i.e., high-viscosity silicone oil, is studied. Direct numerical simulations and a hydrodynamic model based on the lubrication theory are used to support the experimental results.

Findings: Iris opening induces the formation of large circular freestanding films with a stepped profile.

* Corresponding author at: Dipartimento di Ingegneria Chimica, dei Materiali e della Produzione Industriale, Università degli Studi di Napoli Federico II, Piazzale Tecchio 80, 80125 Napoli, Italy.
E-mail address: p.maffettone@unina.it (P.L. Maffettone).
[1] These two authors contributed equally.

https://doi.org/10.1016/j.jcis.2021.03.102

Once iris opening is stopped, the films undergo a capillary leveling flow tending to flatten their profile. The leveling flow follows the theoretical scaling given by Ilton et al. [1]. We prove through numerical simulations that an equi-biaxial extensional flow occurs at the film center. Furthermore, we observe the formation and dynamics of dimples in bare freestanding films for the first time.

1. Introduction

Thin liquid films are of interest in many scientific fields ranging from polymer physics to physiology, biophysics, micro-electronics, surface chemistry, thermodynamics, and hydrodynamics [2,3,4,5,6,7,8,9,10]. In particular, freestanding films, i.e., films with both the surface layers exposed to a different fluid phase (most commonly, a gas), are relevant in the field of foams and emulsions. These were first studied in the form of soap bubbles by Newton [11] and Gibbs [12], yet their formation, stability and break-up are still key issues in the scientific literature [13,1,14,15]. Capillary pressure gradients arise from the local curvature of the free surfaces, leading to liquid rearrangement. If the film is constrained between Plateau borders, the local curvature causes liquid drainage and drives film thinning [16,10]. When the film thickness goes below $\mathcal{O}(10^2)$ nanometers, van der Waals or electrostatic forces generate the so-called disjoining pressure [17], which may drive the film either to break or to find a stable configuration. Destabilization can be triggered by thermal corrugations of the surface layers, which are relevant for very thin films [18,19]. The possible presence of surface-active materials adsorbed on the surface layers strongly affects film dynamics by imparting viscoelastic properties to the interfaces or even leading to surface immobilization [20,21]. On the other hand, surface tension can also smooth out small interfacial perturbations, eventually 'healing' the surface [22]. Recently, capillary leveling flows mediated by viscosity have been analyzed by Ilton et al. [1] on planar freestanding polystyrene films with an initially stepped profile. They prepared a polystyrene film in the glassy state below the glass transition temperature, T_G, and then, upon heating at $T > T_G$, they observed the surface-tension-driven flow of the liquid. They measured the leveling dynamics, i.e., the evolution toward a film of uniform thickness, through atomic force microscopy (AFM) upon cooling the film below T_G. Several heating/cooling cycles for flow at $T > T_G$ and AFM imaging at $T < T_G$ were performed to reconstruct the film thickness dynamics. The most adopted device to form freestanding films and investigate their dynamics under different conditions is the so-called Sheludko cell [16], where a fluid is withdrawn through small tubes at the cell side to form a thin film connected with Plateau borders to a solid wall. Upon cessation of withdrawal, the film freely evolves, draining until break-up or, alternatively, reaching an equilibrium state. In such a device, films with a radius usually around 1 and thickness in the range 50–500 can be formed and studied [10,20].

In this paper, we present a novel opto-mechanical tool combining a customized motorized iris diaphragm and an innovative joint imaging setup complementing digital holography and white light color interferometry that allows to prepare large axisymmetric freestanding liquid films and study their leveling flow. In particular, we form bare (i.e., without surfactants) freestanding circular liquid films with an initial stepped profile made of silicone oil, then we report on liquid leveling flow measured real-time with the aforementioned imaging technique. The film leveling determines equi-biaxial extensional flow conditions at its center. We also show that, during the leveling flow, the formation of dimples can occur at the center of the film. Direct numerical simulations and a hydrodynamic model based on the lubrication theory support the experimental results

2. Materials and methods

2.1. Material

All the experiments are carried out on a pure model Newtonian liquid, namely, silicone oil (PDMS) [14], Dow Corning 200 Fluid, with density $\rho = 976$ kg m^{-3}, kinematic viscosity $\nu = 6 \times 10^{-2}$ m^2 s^{-1}, and surface tension $\gamma = 21.5$ mN m^{-1} at room temperature (25 °C). No surfactants, particles, salts, solvents or other polymers are present in the liquid, so the films can be considered completely bare. Since no concentration or surface tension gradients are expected in the freestanding films, we henceforth consider fully mobile interfaces. Moreover, the fluid is stable at room temperature and has a very low vapor tension, thus hindering evaporation. Heating up of the films can be also considered negligible because the light source used for the interferometric measurements is weak enough to avoid it [23].

2.2. Freestanding film preparation

The formation of a freestanding liquid film with the proper shape to induce leveling flow is a key issue *per se*. We use a stainless steel motorized iris diaphragm (MID), Edmund Optics®, with 16 leaves with thickness 0.2 , vertically oriented symmetry axis, external diameter 70 mm, and maximum aperture 50 mm, operated by a DC gear motor controlled by a programmable circuit board via a pc. The final radius of the iris hole and MID opening/-closing velocity can be fixed at will between 0.5 and 17.5 mm and between 1 and 10 mm s^{-1}, respectively. The film formation (see Fig. 1a) consists in the manual pipetting of a liquid droplet at the center of the closed MID, which has an initial hole radius around 1.1 mm, then, after a resting period of 1–2 min to allow drop shape smoothing, the iris is opened at a constant radial speed up to the desired final hole radius. All the experiments are run at room temperature with final radius $R_0 = 8$ and opening radial velocity $v = 1.5$ mm s^{-1}. It should be remarked that the film radii achievable with this device are one/two orders of magnitude larger than those of the circular films studied so far in the literature [10,20]. Typically, the film thickness at the end of MID opening ranges from 0.15 to 10 depending on the size of the deposited drop. It should be also remarked that the large films formed through the MID have shown to be stable for a sufficient time to observe the leveling phenomenon described below, which is in the order of 10^2. Early film rupture has been never observed except in some rare cases due to the occurrence of external disturbances.

By exploiting the necking induced by the imposed extensional flow [24,25], the MID opening produces a film with a stepped configuration, as qualitatively sketched in Fig. 1b. Some relevant geometrical features are: the thickness $h_T(t)$ of the thinner part at the center of the film, the thickness $h_S(t)$ of the thicker outer region of the film, and the slope $m(t)$ of the step, i.e., the intermediate region. In what follows, subscript 0 will denote values of quantities evalu-

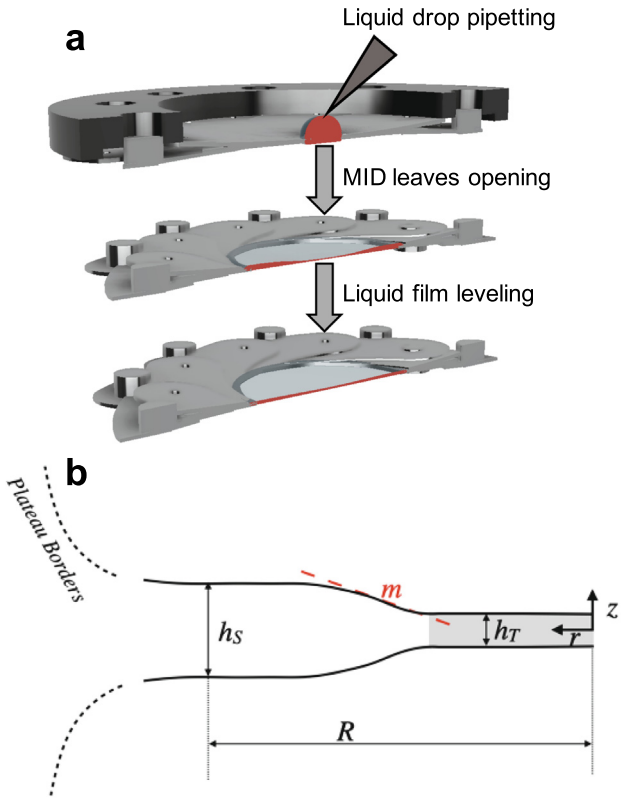

Fig. 1. a: Schematic of material deposition on the iris, iris aperture, and liquid film leveling. b: Qualitative sketch of the side-view profile of the film at the beginning of the leveling flow.

ated at the end of MID opening. This film shape induces a capillary leveling flow driven by surface tension and slowed down by liquid viscous resistance. Such flow conditions hold true until the Plateau border effects come into play, i.e., the outer Plateau borders must be far enough, at least during the initial stages of the leveling phase, to avoid their influence on the dynamics, otherwise, instead of beginning to thicken, the film would carry on thinning even after the end of MID opening, until breaking-up. Furthermore, $h_T(t)$ should be large enough to avoid film destabilization and breakage induced by disjoining pressure (see below) or thickness fluctuations.

We exclude gravitational effects by evaluating the Bond number $\mathrm{Bo} = \Delta\rho g h^2/\gamma < 10^{-5}$, with $\Delta\rho$ the density difference between the two phases (in our case, $\Delta\rho \approx \rho$, i.e., the polymer density), g the gravity acceleration, and h the average film thickness at the end of MID opening. A further check on the irrelevance of gravity is been done by performing numerical simulations by taking gravity into account, whose results are exactly the same as those without gravity reported in *Sec.* 3. We also exclude inertial effects by evaluating the Reynolds number: during MID opening, this can be defined 'conservatively' as $\mathrm{Re} = \rho v R_0/\mu\ 10^{-3}$, with μ the dynamic viscosity of the liquid, whereas, during the leveling phase, it is $\mathrm{Re} = \rho(\gamma/\mu)h/\mu < 10^{-6}$, with γ/μ the capillary velocity [1]. Disjoining pressure effects are also negligible since: *i*) electrostatic contributions are absent as silicone oil molecules are non-polar; *ii*) short-range interactions are relevant on the scale of tens of nanometers, but the films never attains such small thickness values in our experiments; *iii*) by comparing Van der Waals interactions P_σ and capillary pressure Π_W, one obtains $P_\sigma/\Pi_W = (\sigma/\kappa)/(A/(6\pi h^3)) \approx 10^3$, with κ the characteristic curvature, i.e., a time-average of the values calculated through Eq. 5 in the Supporting Information (SI), and $A = 4.4 \times 10^{-20}$ J the Hamaker constant for PDMS [26].

2.3. Interferometric measurement of film thickness

During both the film formation and the leveling flow, the film thickness is measured by an innovative joint imaging method merging digital off-axis holography, based on a Mach-Zehnder interferometer, with white-light color interferometry that allows for the real-time quantitative characterization of freestanding films with high spatial resolution over large areas. The digital holography optical setup is schematized in Fig. 2a and can be described as follows. A laser beam (HeNe emitting at 632.8 nm, exit power 5 mW) is filtered and expanded by the spatial filter SF combined with the lens L1, then it is divided into object and reference beams by the beam splitter BS1. The object beam passes through the film and normally illuminates it, then it is demagnified by the lenses L2 and L3 to fit the aperture of the digital camera CCD (UI-3000SE from IDS). The saturation of the CCD image sensor is avoided by controlling the power of the laser beam with the half-wavelength plate HWP1 together with the polarizing beam splitter PBS. A second beam splitter BS2 allows the interference between reference and object beams in front of the CCD camera. BS2 is slightly tilted so that the two beams overlap with a small angle, which can be controlled in order to adjust the period of the interference fringes. The contrast of the fringes is tuned by polarization and intensity of the interfering beams by using the second half-wavelength plate HWP2, placed into the reference arm of the interferometer, and the variable neutral density filter NDF, placed into the object arm. A color interferometry setup (schematically represented in Fig. 2b) is added. The light of a fluorescent lamp impinges on the film at a 67°-angle and it is reflected towards the second camera CIC (Logitech C920 HD Pro Webcam, 1280x1024px, 30fps). When the film thickness falls into the wavelength range of visible light, a colored region appears (see Fig. 2c). Each color recorded by the webcam corresponds to a thickness of the film through the mathematical relation given by Eq. (2) in Ref. [27]. CCD records digital holograms at 10fps during MID opening and film leveling flow to keep track of the whole process. The field of view (FOV) of the holographic tool is 80 mm^2 around the center of the MID hole. Simultaneously, CIC captures color images like those reported in Fig. 2c and Fig. 5a. Digital holography and white light interferometry 'acquire' the same area of the film and their complementary characteristics are the base of the fusion thickness calculations. More details on such technique are given in *Sec.* 2 in the SI and in the very recent paper by Ferraro et al. [27].

3. Results

3.1. Film formation dynamics

Fig. 3 shows the film thickness dynamics during MID opening for a sample with a volume of about 0.52 μl: the extensional flow stretches the liquid and induces the formation of a film with a thinner central region, where the surface curvature is generally small. It should be remarked that the experimental thickness profiles refer to the central region of the film falling into the FOV of the optical setup and are obtained by averaging each datum over a 70-μm-long radial range. At the end of MID opening, the film central portion has a similar shape to that sketched in Fig. 1b. The film thickness profile can be tuned by changing the initial amount of fluid or/and MID opening radius.

Since the experimental thickness profiles are limited to the film central region, direct numerical simulations are implemented to investigate the complete thickness profile induced by the MID

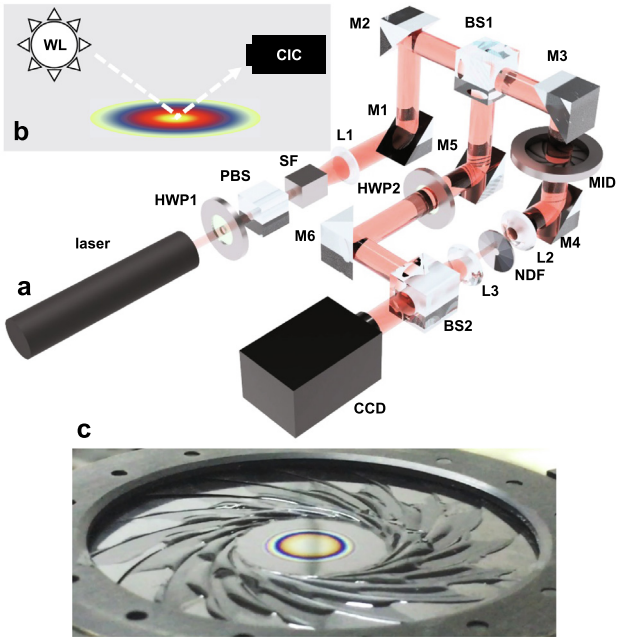

Fig. 2. a: Setup for thin liquid film thickness holographic measurement (SF: spatial filter; M1-M4: mirrors; HWP1-HWP2: half-wavelength plates; PBS: polarizing beam splitter; BS1-BS2: beam splitters; L1-L3: lenses; NDF: neutral density filter; MID: iris diaphragm with the polymer inside; CCD: digital camera). b: Schematic of the color interferometry setup. c: Typical image observed by CIC during the experimental campaign.

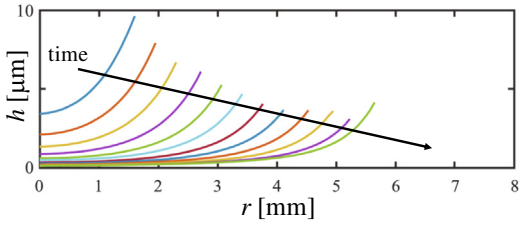

Fig. 3. Experimental radial profiles of the thickness of the film during MID opening for a sample with a volume of about 0.52 μl.

opening. The motion equations for a Newtonian liquid with fully mobile gas–liquid interfaces and neglecting inertia (Stokes flow) are solved with a finite-element method (FEM). The mathematical model underlying FEM simulations and the details on the numerical technique are given in *Sec.* 3 in the SI. Fig. 4a1 depicts the geometry considered in the simulations before MID opening is started. When the MID is 'closed', its hole has radius $R_c = 1$ mm, whereas the thickness of the liquid drop at the center of the hole is $h_d = 2$ mm. The thickness of the lamellae is $h_L = 0.2$ mm. A cylindrical coordinate system is used and we impose both axial symmetry and top-down planar symmetry due to the irrelevance of gravity suggested by vanishing Bo and expected fast equilibration driven by pressure [28]. As a further verification of the irrelevance of gravity, some simulations are performed on a complete domain with no top-down symmetry by taking gravity into account, whose results overlap completely those without gravity. The lamellae move with constant velocity $v = 1.5$ mm s^{-1} until the MID hole reaches its final radius R_0, as shown in panel a2 for a ratio between the final and the initial radius of the hole of the MID $R_0/R_c = 8$. The central part of the film 'necks' during MID opening, thus determining a sigmoidal stepped geometry where the film is thin and almost flat in a wide region around its center, with thickness h_0, then its thickness steeply increases in the radial direction approaching the iris lamel-

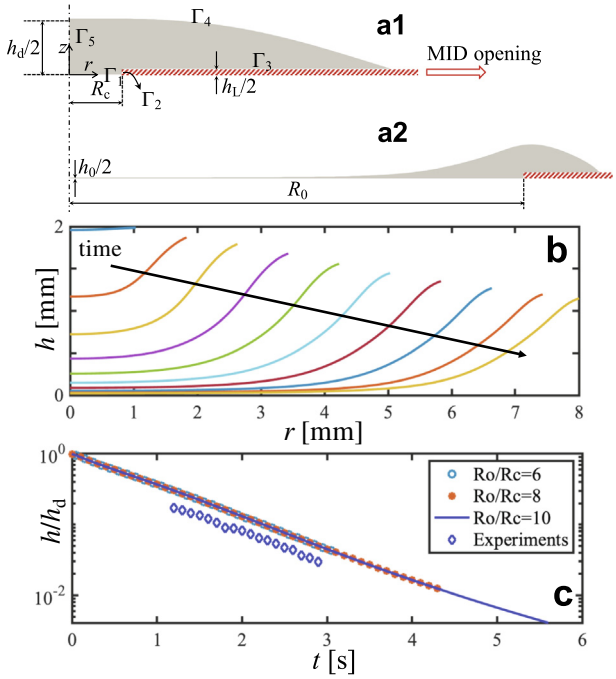

Fig. 4. a: Sketch of the computational domain for direct numerical simulations of film stretching and leveling with reference to MID opening start (b1) and stop (b2) for $R_0/R_c = 8$. b: Calculated radial thickness profiles of the film during MID opening for $R_0/R_c = 8$. c: Numerical and experimental time evolution of the thickness of the film at its center during MID opening.

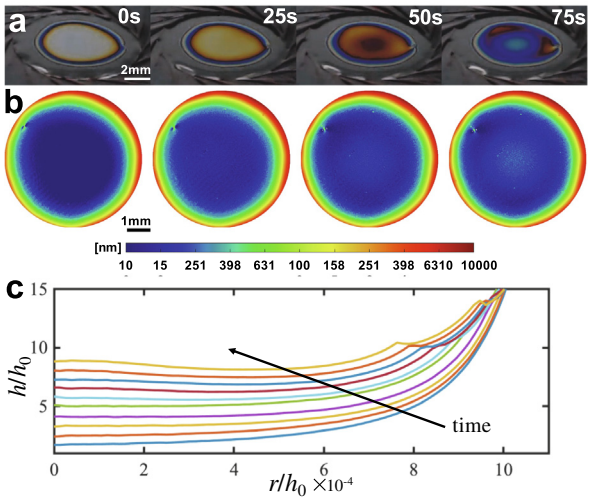

Fig. 5. a: Concentric colored fringes generated by white light interferometry. b: Thickness map measured with holographic microscopy. c: Experimental thickness profile evolution during early stages of the leveling flow (see time–values in panel a) with $h_0 = 60$ nm.

lae. Fig. 4b shows the numerically computed film stretching dynamics for the geometry shown in Fig. 4a. The qualitative agreement between the numerical and the experimental results in Fig. 3 is remarkable, yet quantitative differences arise that can be attributed to the fact that the experimental initial condition cannot be so 'clean' and regular as that considered in numerical simulations. In addition, the experimental curves only represent the 'left part' of the numerical ones due to the finiteness of the FOV of the optical tool, which is not an issue in the numerical case. The effect on film stretching of changing the MID aperture is reported in Fig. 4c, where we display the temporal history of the thickness at the cen-

ter of the film, normalized by its initial value, for three values of R_0/R_c considered in the simulations and for the experimental case shown in Fig. 3. Of course, since an inertialess Newtonian liquid is considered, the numerical curves superimpose and stop at increasingly longer time at increasing R_0/R_c. Noteworthy, the agreement with the experimental data is very good, thus confirming that our direct numerical simulations can effectively describe the actual film formation dynamics.

3.2. Leveling flow

The time evolution of the film thickness during the leveling flow is displayed in Fig. 5. Fig. 5a shows the color fringes: as the thickness of the central part of the film reaches the wavelength of the visible light, interference colors become visible in white light, then they change in time following the film thickness dynamics. At early time ($t < 50$ s), the colored region is almost circular and the fringes inside it move from the periphery to the center. At longer time, the effects of the regions close to the lamellae become relevant and the axial symmetry is lost (see the fourth snapshot in Fig. 5a). Fig. 5b reports the maps of film thickness at different times from holography, whereas the film thickness radial profiles are given in Fig. 5c, showing progressive film flattening. In addition, from both the last two snapshots in Fig. 5b and the last profiles in Fig. 5c the formation of a dimple at the center of the film is visible (see *Sec.* 3.3).

The FOV accessible with holography allows for the observation of the film intermediate region and the quantitative measurement of its slope m (see Fig. 1b). Fig. 6a reports $m(t)$ in log scale at intermediate times for several experiments with different initial amounts of liquid. This is an example of the intermediate asymptotic behavior of capillary-driven flow in thin films [29]. As it is apparent, $m(t)$ always follows a power-law decay with exponent $-1/2$, in agreement with the predictions by Ilton et al. [1]. Different positions of the data sets are due to different initial amounts of liquid from one experiment to another. Fig. 6b reports the slope values obtained from direct numerical simulations with different values of R_0/R_c, whose agreement with experiments is excellent. Like in Ilton et al. [1], the scaling can be validated with a model based on the lubrication long-wave theory, which makes use of the Young-Laplace equation in the small-slope approximation with negligible inertia, constant viscosity and surface tension, and no-shear boundary conditions at each liquid–air interface. After derivation in axisymmetric geometry, given in *Sec.* 4 in the SI, the model reads

$$\begin{aligned} &h_t + \tfrac{(rhu)_r}{r} = 0, \\ &\left[\tfrac{(rh_r + 3ru)_r}{r}\right]_r + \tfrac{2h_r}{h}\left[\tfrac{(ru)_r}{r} + u_r\right] = 0. \end{aligned} \tag{1}$$

Notice that all the quantities appearing in Eq. (1) are dimensionless, the usual superscript * being omitted for brevity. The scales are h_{T0} for lengths and $h_{T0}\mu/(\gamma\varepsilon^2)$ for time, with $\varepsilon = h_{T0}/R$. The dimensionless film thickness h and radial velocity u only depend on time t and radial direction r. The subscripts $_t$ and $_r$ denote derivatives with respect to these variables. The derivation follows Munch et al. [30] for the free-slip limit, yet with an axisymmetric geometry. Once linearized at the lowest order in the small parameter h_{T0}/R, the thickness dynamics obeys a diffusive-like equation and, at this order, the slope $m(t)$ decreases at intermediate times with $t^{-1/2}$.

In view of the good agreement between experiments and finite-element simulations, the numerical results can be safely used to characterize the flow conditions at the film center. Fig. 7a reports the time evolution of the dimensionless thickness at the center of the film during the leveling flow. From these data, we compute the strain rate $\dot{\varepsilon} = \|-1/(2h)dh/dt\|$. The stress difference $\|T_{zz} - T_{rr}\|$ at $r = 0$ can be also extracted from the numerically computed stress fields. Fig. 7b shows the dimensionless stresses versus the dimensionless strain rate. It can be observed that, depending on the extent of MID hole aperture, different ranges of strain rate

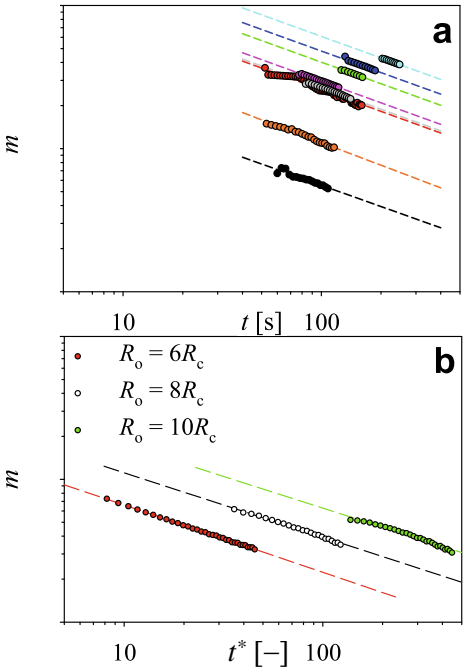

Fig. 6. Time evolution of the slope m of the film intermediate region. a: Experimental results for experiments with different initial amounts of liquid. b: Numerical results for three different values of MID hole opening radius (time scale $2h_0\mu/\gamma$). Dashed lines are power laws $\propto 1/\sqrt{t}$.

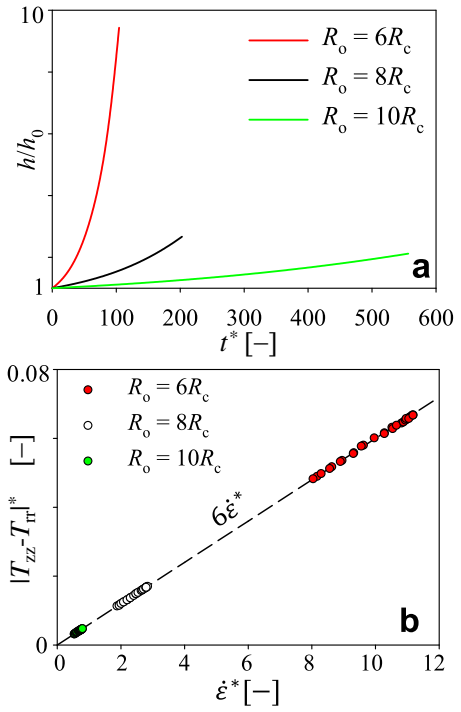

Fig. 7. a: Calculated time evolution of the thickness at the center of the film during leveling flow (time scale $2h_0\mu/\gamma$). b: Calculated dimensionless stress difference $\|T_{zz} - T_{rr}\|^*$ (stress scale γ/h_0) at the center of the film as a function of the dimensionless strain rate $\dot{\varepsilon}^*$. The dashed line reports the prediction for equi-biaxial extensional flow of a Newtonian liquid. In both panels, three values of the ratio R_0/R_c are considered, as reported in the legend.

are explored at the center of the film during leveling, the more the MID hole is opened the lower the strain rate during leveling. Furthermore, numerical simulations prove that at the film center the flow conditions are those of an equi-biaxial extensional flow, as the data obey the law $\|T_{zz} - T_{rr}\| = 6\mu\dot{\varepsilon}$ characterizing the equi-biaxial extensional flow of a Newtonian liquid.

3.3. Dimple formation during leveling flow

The film thickness holographic maps and profiles in Fig. 5 show the formation of a dimple, also known as 'bump', namely, a local thickness maximum at the center of the film that induces a change of concavity in the film thickness radial profile. According to our experimental observations, this happens when h_0 is below a critical value ≈ 250 nm at the end of MID opening. Fig. 8 displays an example of the two different scenarios appearing in the experiments, i.e., film capillary leveling without dimple formation for $h_0 = 650$ nm (a) and with dimple formation for $h_0 = 250$ nm (b). In planar freestanding films, bumps cannot form during leveling flows [1], whereas, in confined axisymmetric films, mass conservation might cause fluid accumulation near the center of the film resulting in bump appearance. Film thickness profile at the beginning of the leveling phase is also relevant for the formation of dimples. Indeed, by looking at the initial thickness profiles (the blue curves) in Fig. 8, it can be seen that, when the dimple does not form (a), the film thickness increases 'earlier' in the radial direction than when the dimple forms (b), where the almost flat region around the center of the film has a larger radial extent. As a further proof, we solve the lubrication model, Eq. (1), by choosing two different initial sigmoidal profiles and imposing symmetry boundary conditions at $r = 0$ and $u = 0$, $h_r = 0$, and $h_{rr} = 0$ at $r = R$ (so excluding the Plateau borders from the picture). Consistently with the experimental observations, the dimple is absent in the case where the initial film profile increases closer to the center (see Fig. 9a), whereas it readily appears where the flat central region is initially more extended (see Fig. 9b). The different scenarios might be attributed to the different 'graduality' of the curvature change from the central to the outer film region. The initial concavity of the profile in the central region is such that the liquid should move towards the outer region, whereas that in the outer region plays in the opposite direction: the relative importance of the two contributions determines the observed dynamics. It should be remarked that, in our lubrication model, the capillary flow does only depend on surface tension effects, no effect of disjoining pressure being taken into consideration.

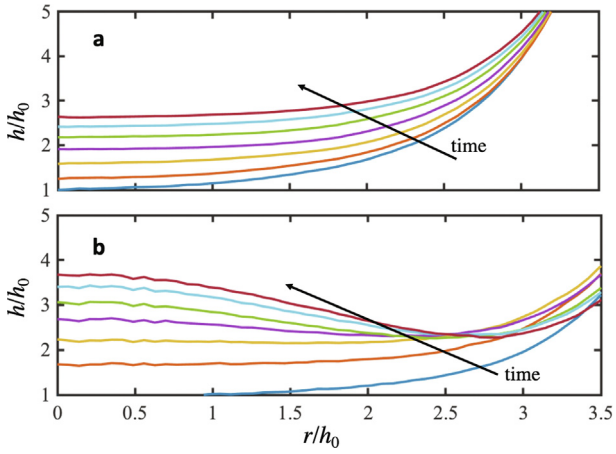

Fig. 8. Experimental film thickness dynamics without dimple formation for $h_0 = 450$ nm (a) and with dimple formation for $h_0 = 250$ nm (b).

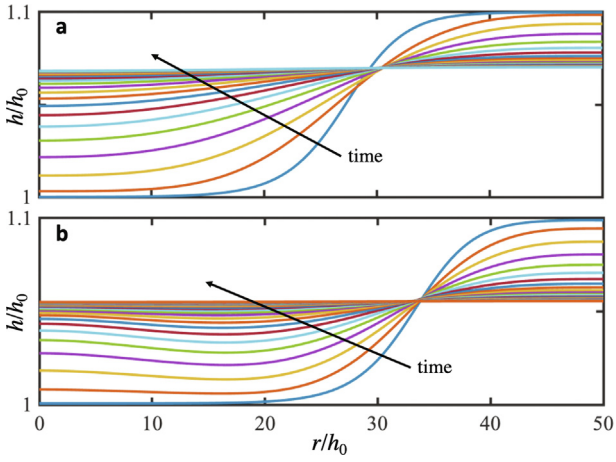

Fig. 9. Numerical solutions of the model based on the lubrication theory, Eq. (1). a: Dynamics without dimple formation. b: Dynamics with dimple formation. The initial profiles are the blue sigmoidal curves at earliest time. (For interpretation of the references to color in this figure legend, the reader is referred to the web version of this article.)

4. Final remarks

In this paper, we present a novel opto-mechanical tool to generate stable large circular bare freestanding liquid films with a motorized iris diaphragm (MID) and study their dynamics in real time with a joint imaging method combining digital holography and white-light color interferometry that gives detailed time-resolved data on film thickness over a large field of view. After iris opening, the films attain a stepped profile and undergo a leveling flow tending to flatten it. The model Newtonian liquid material used in our experiments, i.e., PDMS, is transparent, which makes it extremely suitable for digital holography. However, it should be said that the opacity of many other polymers in their bulk form would not be a significant experimental issue, because, when thin films are considered, these are always at least partially transparent to the visible light. In addition, if the transmitted light intensity is much weaker than the incident light intensity, the latter could be properly increased to adjust the signal and obtain a good measure.

The experimental findings are validated through direct numerical simulations and a model based on the lubrication theory in the same line of the results by Ilton et al [1]. At variance with them, we have an approximately circular film and, above all, in our experiments the polymer is always well above its glassy transition temperature and the film dynamics is measured real-time without the need of cooling and annealing. The equi-biaxial nature of the leveling flow field at the film center detected through numerical simulations might open the perspective of using the device to measure the equi-biaxial extensional viscosity of liquids, a usually quite elusive quantity whose measurement is very difficult to achieve. It is worth specifying that a direct measurement of stresses is not mandatory to this aim, since arguments analogous to the ones underlying the project equation of the Capillary Breakup Extensional Rheometer (CaBER) [31] for uniaxial extensional viscosity could be exploited to retrieve the value of the ratio between the surface tension and the liquid viscosity from the observation of the time evolution of the film thickness profile. (The details of such analysis go beyond the scope of this paper and will be given elsewhere.) There are, of course, practical limitations on the accessible strain rates, but the experimental window can be widened by

properly tuning MID opening. On the other hand, the manual operation of the MID and the inherent inhomogeneity of the wetting of its leaves represent a critical aspect of the proposed method and work has to be done to optimize the tool.

Finally, MID could be also used for analyzing decorated films and films with deposited particles, which could reveal very useful in understanding the role of particles in stabilizing foams and emulsions [15].

Declaration of Competing Interest

The authors declare that they have no known competing financial interests or personal relationships that could have appeared to influence the work reported in this paper.

Acknowledgement

PLM thanks Howard A. Stone for fruitful discussions. The research has been partly funded by project PRIN 2017, Morphological Biomarkers for early diagnosis in Oncology (MORFEO) Prto. 2017N7R2CJ, and MIUR PON Project 2014-2020 PROSCAN.

Appendix A. Supplementary data

Supplementary data to this article can be found online at https://doi.org/10.1016/j.jcis.2021.03.102.

References

[1] M. Ilton, M.P. Couchman, C. Gerbelot, M. Benzaquen, P.D. Fowler, H.A. Stone, E. Raphaël, K. Dalnoki-Veress, T. Salez, Capillary leveling of freestanding liquid nanofilms, Phys. Rev. Lett. 117 (2016) 1–5.
[2] A. Sharma, E. Ruckenstein, Stability, critical thickness, and the time of rupture of thinning foam and emulsion films, Langmuir 3 (5) (1987) 760–768.
[3] R. Aveyard, J.H. Clint, Foam and thin film breakdown processes, Curr. Opin. Colloid Interface Sci. 1 (1996) 764–770.
[4] E. Ruckenstein, C. Dunn, Stability of thin solid films, Thin Solid Films 51 (1978) 43–75.
[5] A. Constantinescu, L. Golubovic', A. Levandovsky, Beyond the young-laplace model for cluster growth during dewetting of thin films: Effective coarsening exponents and the role of long range dewetting interactions, Physical Review E 88 (3) (2013) 032113.
[6] J.D. McGraw, N.M. Jago, K. Dalnoki-Veress, Capillary levelling as a probe of thin film polymer rheology, Soft Matter 7 (2011) 7832–7838.
[7] G. Singh, C. A. Miller, H. G. J., On dimple formation in foam films, J. Coll. Interface Sci. 187 (1997) 334-337.
[8] G. Debrégeas, P.-G. de Gennes, F. Brochard-Wyart, The life and death of 'bare' viscous bubbles, Science 279 (1997) 1704–1707.
[9] G. Debrégeas, P. Martin, F. Brochard-Wyart, Viscous bursting of suspended films, Phys. Rev. Lett. 75 (1995) 3886–3889.
[10] D.Y.C. Chan, E. Klaseboer, R. Manica, Film drainage and coalescence between deformable drops and bubbles, Soft Matter 7 (2011) 2235–2264.
[11] I. Newton, Optics, Vol. Part II Experiment IV, The Royal Society, London, 1704.
[12] J. W. Gibbs, On the equilibrium of heterogeneous substances, Trans. Connecticut Acad. Arts Sci. 3 (May 1877 - July 1878) 343-524.
[13] M. Rivetti, T. Salez, M. Benzaquen, E. Raphaël, O. Baümchen, Universal contact-line dynamics at the nanoscale, Soft Matter 11 (2015) 9247–9253.
[14] L. Champougny, E. Rio, F. Restagno, B. Scheid, The break-up of free films pulled out of a pure liquid bath, J. Fluid Mech. 811 (2017) 499–524.
[15] A. Yadav, E. J. Hinch, M. S. Tirumkudulu, Capillary-induced motion of particles bridging interfaces of a free-standing thin liquid film, Phys. Rev. Lett. 122 (098001).
[16] A. Sheludko, Thin liquid films, Adv. Colloid Interface Sci. 1 (1967) 391–464.
[17] B.V. Derjaguin, The definition and magnitude of disjoining pressure and its role in the statics and dynamics of thin fluid films, Kolloid Zh. 17 (1955) 205–214.
[18] D. Langevin, C. Marquez-Beltran, J. Delacotte, Surface force measurements on freely suspended liquid films, Adv. Coll. Interface Sci. 168 (2011) 124–134.
[19] S.I. Karakashev, E.D. Manev, Hydrodynamics of thin liquid films: Retrospective and perspectives, Adv. Coll. Interface Sci. 222 (2015) 398–412.
[20] J.E. Coons, P.J. Halley, S. McGlashan, T. Tran-Cong, A review of drainage and spontaneous rupture in free standing thin films with tangentially immobile interfaces, Adv. Coll. Interface Sci. 105 (2003) 3–62.
[21] A. Choudhury, V.K. Paidi, S.K. Kalpathy, H.N. Dixit, Enhanced stability of free viscous films due to surface viscosity, Physics of Fluids 32 (8) (2020) 082108.
[22] M. Backholm, M. Benzaquen, T. Salez, E. Raphaël, K. Dalnoki-Veress, Capillary levelling of a cylindrical hole in a viscous film, Soft Matter 10 (2014) 2550–2558.
[23] B. Mandracchia, Z. Wang, V. Ferraro, M.M. Villone, E. Di Maio, P.L. Maffettone, P. Ferraro, Quantitative imaging of the complexity in liquid bubbles' evolution reveals the dynamics of film retraction, Light: Science & Applications 8 (1) (2019) 20.
[24] D.M. Hoyle, S.M. Fielding, Necking after extensional filament stretching of complex fluids and soft solids, J. Non-Newt. Fluid Mech. 247 (2017) 132–145.
[25] J. Seiwert, M. Monloubou, B. Dollet, I. Cantat, Extension of a suspended soap film: A homogeneous dilatation followed by new film extraction, Phys. Rev. Lett. 111 (094501).
[26] J. Israelachvili, Intermolecular and Surface Forces, Academic Press, 2011.
[27] V. Ferraro, Z. Wang, L. Miccio, P.L. Maffettone, Full-field and quantitative analysis of a thin liquid film at the nanoscale by combining digital holography and white light interferometry, The Journal of Physical Chemistry C 125 (2021) 1075–1086.
[28] V. Bertin, J. Niven, H.A. Stone, T. Salez, E. Raphael, K. Dalnoki-Veress, Symmetrization of thin freestanding liquid films via a capillary-driven flow, Physical Review Letters 124 (18) (2020) 184502.
[29] M. Benzaquen, T. Salez, E. Raphaël, Intermediate asymptotics of the capillary-driven thin-film equation, Eur. Phys. J. E 36 (82) (2013) 1–7.
[30] A. Munch, B. Wagner, W. T.P., Lubrication models with small to large slip lengths, Journal of Engineering Mathematics 53 (2005) 359-383.
[31] G.H. McKinley, A. Tripathi, How to extract the newtonian viscosity from capillary breakup measurements in a filament rheometer, Journal of Rheology 44 (3) (2000) 653–670.